

Toward Large-Scale Energy Harvesting by a Nanoparticle-Enhanced Triboelectric Nanogenerator

Guang Zhu,^{†,§} Zong-Hong Lin,^{†,§} Qingshen Jing,[†] Peng Bai,[†] Caofeng Pan,^{†,‡} Ya Yang,[†] Yusheng Zhou,[†] and Zhong Lin Wang^{*,†,‡}

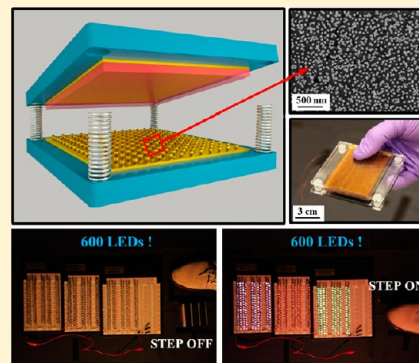
[†]School of Material Science and Engineering, Georgia Institute of Technology, Atlanta, Georgia 30332-0245, United States

[‡]Beijing Institute of Nanoenergy and Nanosystems, Chinese Academy of Sciences, Beijing, China

S Supporting Information

ABSTRACT: This article describes a simple, cost-effective, and scalable approach to fabricate a triboelectric nanogenerator (NG) with ultrahigh electric output. Triggered by commonly available ambient mechanical energy such as human footfalls, a NG with size smaller than a human palm can generate maximum short-circuit current of 2 mA, delivering instantaneous power output of 1.2 W to external load. The power output corresponds to an area power density of 313 W/m² and a volume power density of 54 268 W/m³ at an open-circuit voltage of ~1200 V. An energy conversion efficiency of 14.9% has been achieved. The power was capable of instantaneously lighting up as many as 600 multicolor commercial LED bulbs. The record high power output for the NG is attributed to optimized structure, proper materials selection and nanoscale surface modification. This work demonstrated the practicability of using NG to harvest large-scale mechanical energy, such as footsteps, rolling wheels, wind power, and ocean waves.

KEYWORDS: Triboelectric nanogenerator, large-scale, nanoparticle, wind power, ocean wave



We are surrounded by enormous amounts of ambient mechanical energy that goes to waste such as rain drops, human footfalls, air flow, and ocean waves, just to name a few. Research on mechanical energy harvesting falls into three established categories, that is, electrostatic,^{1,2} piezoelectric,^{3–6} and electromagnetic.^{7,8} It has been mainly focused on small-scale energy harvesting, aiming at powering micro/nano-systems^{9–11} for applications including sensors,^{12,13} environmental monitoring,¹⁴ medical science,^{15,16} personal electronics,^{17,18} and defense technology.¹⁹ With the advances in technology developed for small-scale energy harvesting, it may be possible to scale up this type of technology at a large scope^{1,10} such as with ocean waves²⁰ and wind power.²¹ Such potential needs to be explored with a consideration of the scalability of the technology, the cost of materials and fabrication process, environmental impact, and practical feasibility for implementation.

The triboelectric effect is an old phenomenon and is usually undesirable because of potential hazards to electronics and public safety. However, it has recently been utilized as an extremely effective means to harvest mechanical energy by a new type of organic/polymer nanogenerators (NG).^{21–23} Energy conversion is achieved by coupling between the triboelectric effect and the electrostatic effect. Contact between two materials that differ in polarity of triboelectricity yields surface charge transfer. As they separate, a dipole moment is established, driving electrons through external loads. The NG acts as a charge-pump, in which current flows back and forth between the electrodes in alternating current (AC) character-

istics.²¹ It provides an unprecedentedly simple and cost-effective means of harvesting ambient mechanical energy mainly using polymer-based materials.

Here in this work, we developed a new triboelectric NG that has not only much simplified structure but also substantially higher power output enabled by nanoparticle-based surface modification. The short-circuit current reached a peak value of 2.0 mA, which corresponded to the instantaneous power output of 1.2 W and power density of 313 W/m². The average power output and energy conversion efficiency at device level were calculated to be 132.1 mW and 9.8%, respectively. For the first time, we experimentally realized scaling up of the NG's power output, making it power not just a single electronic device but hundreds of them simultaneously. Triggered by commonly available mechanical source such as footfalls, the NG was capable of instantaneously lighting up 600 commercial LED bulbs in real time at an estimated output open circuit voltage of ~1200 V. This work unravels the practicability of harvesting mechanical energy by the NG on a large scale. The working mechanism demonstrated here can be further applied to potentially harvesting large-scale mechanical energy such as rolling wheels, wind power, and ocean waves.

The NG has a layered structure with two substrates, as schemed in Figure 1a. Poly(methyl methacrylate) (PMMA)

Received: January 9, 2013

Revised: January 23, 2013

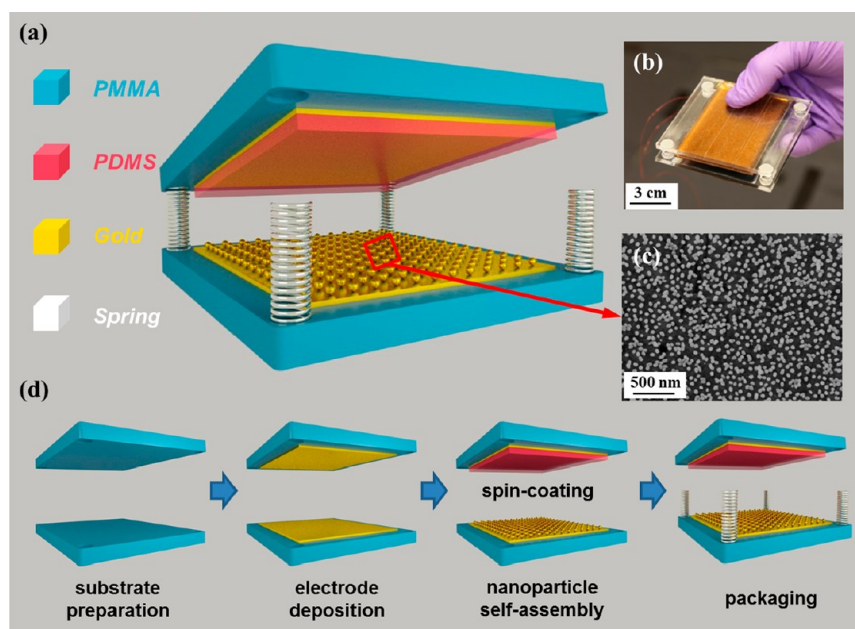


Figure 1. (a) Schematic and (b) photograph of a fabricated triboelectric NG. (c) SEM image of gold nanoparticles coated on gold surface. (d) Process flow for fabricating the NG.

was selected as the material for substrates due to its decent strength, light weight, easy processing, and low cost. On the lower side, a layer of contact electrode is prepared. The contact electrode plays dual roles of electrode and contact surface. It consists of a gold thin film and gold nanoparticles coated on the surface. Alternatively, nanoparticles of nonprecious metals can also be used as replacements. Figure 1c shows the uniform distribution of the nanoparticles on the surface. They modify the surface both physically and chemically, which will be discussed in detail later. On the other side, a thin film of gold is laminated between the substrate and a layer of polydimethylsiloxane (PDMS). This electrode is called a back electrode for later reference. The two substrates are connected by four springs installed at the corners, leaving a narrow spacing between the contact electrode and the PDMS. The as-fabricated NG is exhibited in Figure 1b. As sketched in Figure 1d, the fabrication flow is straightforward without sophisticated equipment and process. Detailed fabrication specifications are discussed in the Methods section.

The electric energy generation process can be explained by the coupling between triboelectric effect and electrostatic effect, as sketched in Figure 2. At original position, a separation distance is maintained by springs, as indicated by d_0 in Figure 2a. When an external impact is applied on one of the substrates, gold and PDMS are brought into contact. According to the triboelectric series that ranks materials' tendency to gain or lose electrons, electrons are injected from gold into PDMS,^{24–26} resulting in surface triboelectric charges (Figure 2b),^{27,28} which are retained on the PDMS. As the impact is withdrawn, the contacting surfaces move apart due to restoring force from the springs. Once a separation forms, the back electrode possess a lower electric potential than the contact electrode, producing an electric potential difference. Such a potential difference drives electrons through external loads and screens the positive triboelectric charges on the contact electrode (Figure 2c). When the NG reverts back to the original position, positive triboelectric charges on the contact electrode are completely screened, leaving an equal amount of inductive charges on the

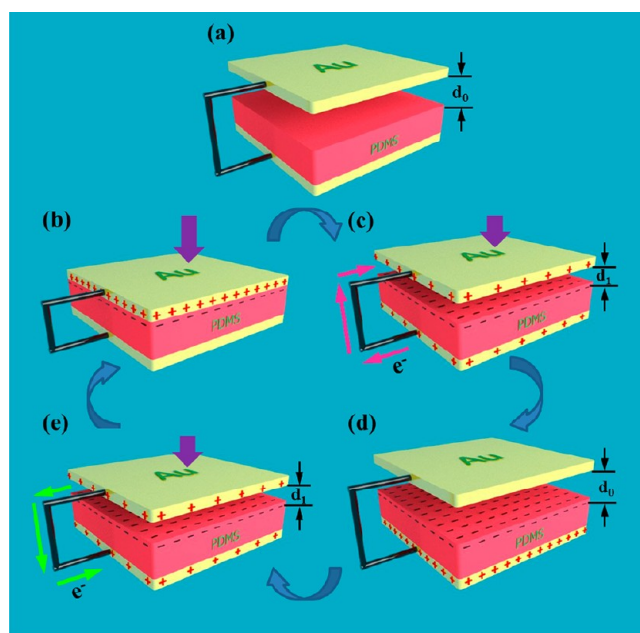


Figure 2. (a) Original position without mechanical force applied. (b) External force brings gold and PDMS into contact, generating positive triboelectric charges on the gold side and negative charges on the PDMS side. (c) Withdrawal of the force causes a separation. Potential difference drives electrons from the back electrode to the contact electrode, screening the triboelectric charges and leaving behind inductive charges. (d) Original position is recovered with all positive triboelectric charges screened on the contact electrode. (e) Electrons are driven back to the back electrode as the force is reapplied, screening the inductive charges. Note: For simplification, nanoparticles and springs are not shown in the schematics.

back electrode (Figure 2d). Subsequently, mechanical impact once again shortens the separation, producing an electric potential difference with reversed polarity. In consequence, electrons flow in a reversed direction (Figure 2e). They keep screening inductive charges on the back electrode until a direct

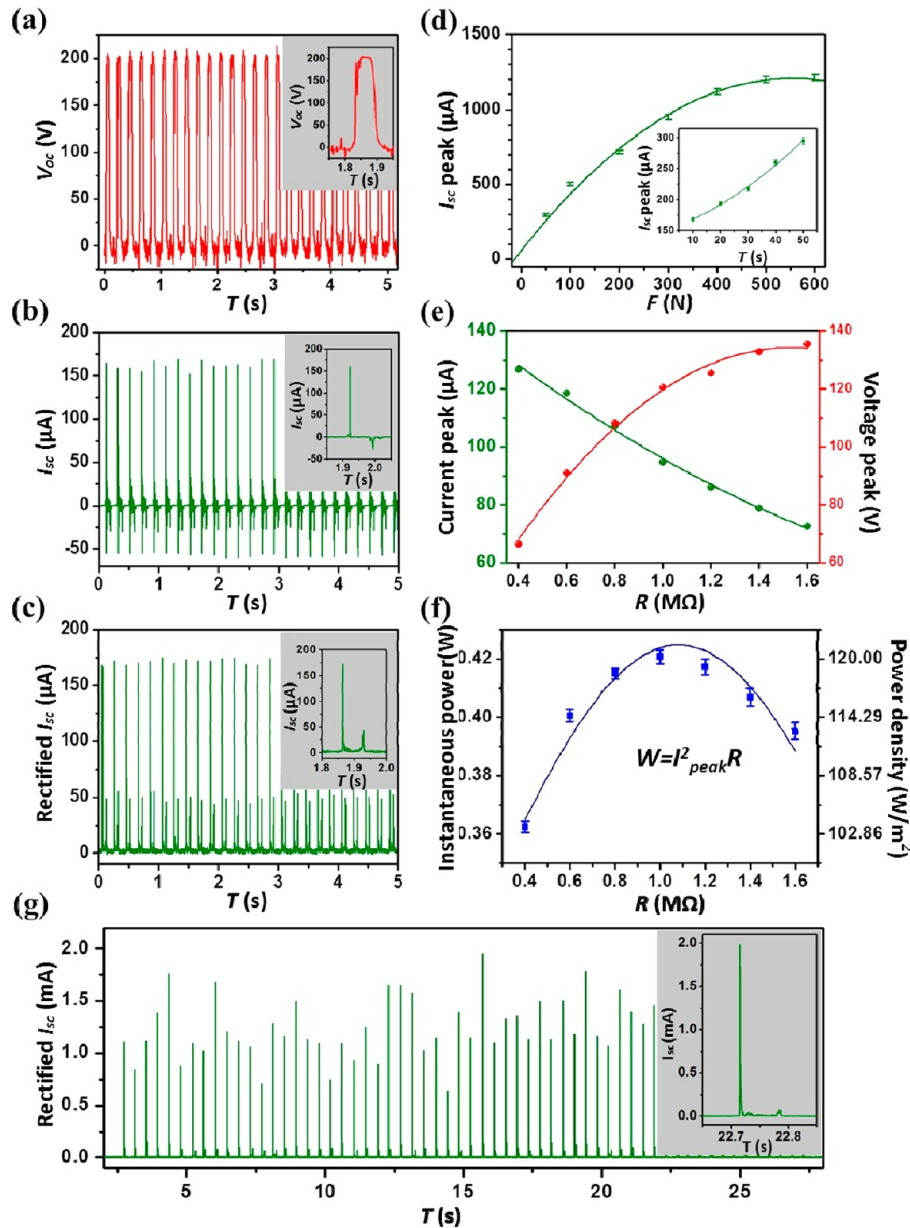


Figure 3. (a) Open-circuit voltage (V_{oc}) at contacting force of 10 N. Inset: enlarged view of one cycle. Separation causes rising of the V_{oc} to a plateau value and contact make it fall back to zero. (b) Short-circuit current (I_{sc}) at contacting force of 10 N. Inset: enlarged view of one cycle. Contact and separation correspond to a positive current pulse and a negative current pulse, respectively. (c) Rectified short-circuit current (I_{sc}) by a full-wave bridge at contacting force of 10 N. Inset: enlarged view of one cycle, showing two current pulses in the same direction. (d) Dependence of the I_{sc} on the contacting force. The larger contacting force corresponds to higher current until saturation occurs. Inset: I_{sc} at contacting force less than 50 N. The data points represent the peak value of current pulses while the line is the fitted result. (e) Dependence of the current output on external load resistance at contacting force of 10 N. Increased load resistance results in lower current output but higher voltage output. The points represent peak value of electric signals while the line is the fitted result. (f) Dependence of the power output on external load resistance at contacting force of 500 N, indicating maximum power output when $R = 1 \text{ M}\Omega$. The curve is a fitted line. (g) Short-circuit current (I_{sc}) when triggered by human footfall that can generate contacting force between 500 and 600 N. Inset: enlarged view of the highest current pulse.

contact is again established (Figure 2b). It is to be noted that the insulating PDMS allows long-time retention of the triboelectric charges on its surface²⁹ even through the triboelectric charges on the metal side are periodically screened by inductive charges. In this process, the NG acts as an electron pump that drives electrons back and forth between the two electrodes.²¹

To trigger the NG, a mechanical shaker was used to apply impulse impact. Here, the interaction force generated between the gold and the PDMS is defined as contacting force, which

was monitored by a force sensor (Supplementary Figure S1). Open-circuit voltage (V_{oc}) and short-circuit current (I_{sc}) were measured to characterize the NG's electric performance. With a contacting force of 10 N, the V_{oc} and the I_{sc} are presented in Figure 3a and b, respectively. The V_{oc} switched between zero and a plateau value, respectively corresponding to the contact position and the original position. The I_{sc} exhibits AC behavior, with an equal amount of electrons flowing in opposite directions within one cycle (Supplementary Figure S2). The experimental data validate the working principle described in

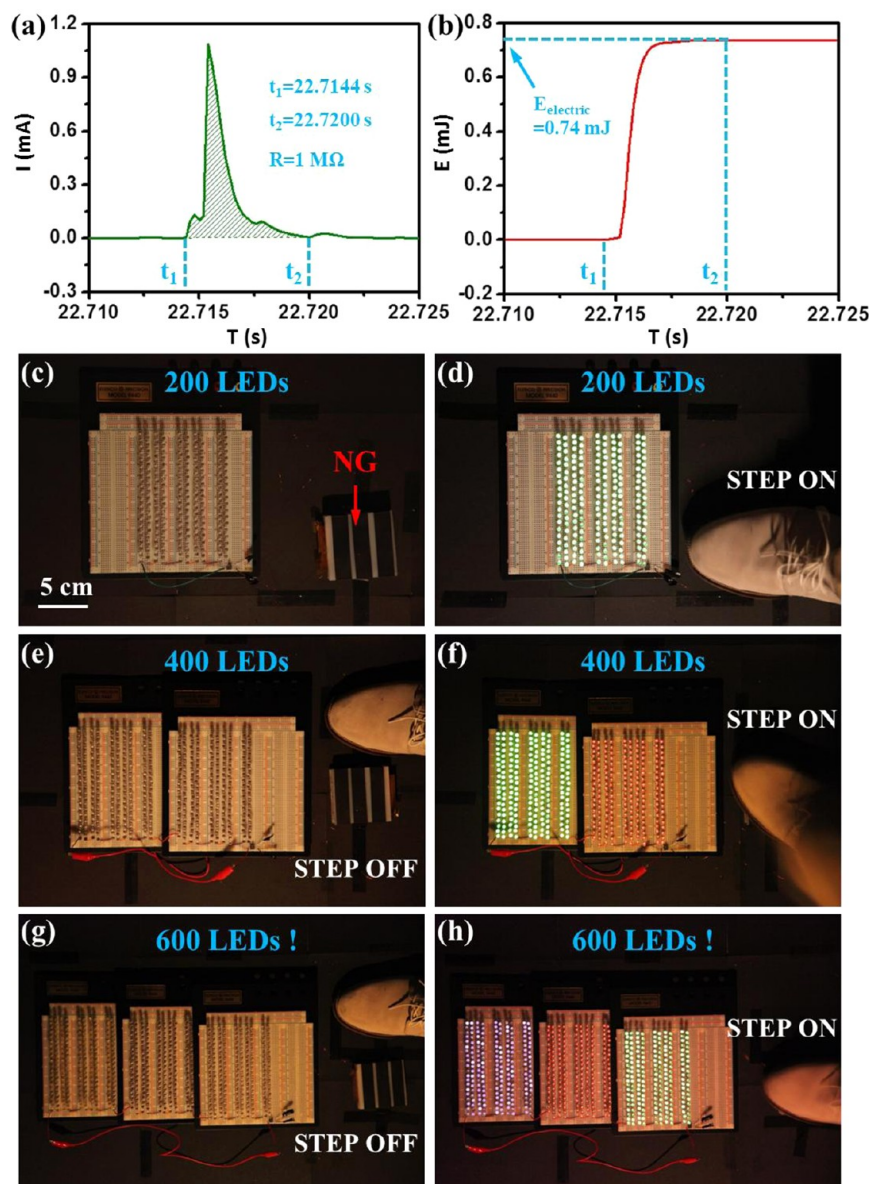


Figure 4. (a) A current pulse output produced by human footfall at load resistance of $1\text{ M}\Omega$ when a contact is made. (b) Electric energy generated by the current pulse in part a, which is equal to the Joule heating from the resistor of $1\text{ M}\Omega$. (c) Photograph of a setup in which the NG acts as a direct power source for 200 commercial green LED bulbs and (d) when footstep falls on the NG, simultaneously lighting up the LEDs in real-time. (e) Photograph of a setup in which the NG acts as a direct power source for 200 commercial green and red LED bulbs, respectively, and (f) when footstep falls on the NG, simultaneously lighting up the LEDs in real time. (g) Photograph of a setup in which the NG acts as a direct power source for 200 commercial green, red and blue LED bulbs, respectively and (h) when footstep falls on the NG, simultaneously lighting up the LEDs in real time. The estimated output open circuit voltage is $\sim 1200\text{ V}$. Note: all LEDs are connected in serial.

Figure 2. It is observed that the current signal for separation has a smaller magnitude but longer duration than that for contact (inset of Figure 3b). It can be explained by faster contact resulting from external impact compared to slower separation caused by restoring force of the springs. The polarity of the measured electric signals can be reversed upon switching the connection polarity between the NG and the measurement instrument (Supplementary Figure S3). Furthermore, the AC output could be transferred to pulse output in the same direction simply by a full-wave rectifying bridge (Figure 3c).

The NG's electric output is strongly related to the contacting force, yielding higher output with larger force. At a force as small as 10 N , the NG can still produce I_{sc} ranging from $160\text{ }\mu\text{A}$ to $175\text{ }\mu\text{A}$ (Figure 3d). When the force increases to 500 N , the

electric output reaches a saturated value, producing a peak I_{sc} of 1.2 mA . This result is due to increased contact area with larger force. The two contacting surfaces are neither absolutely flat nor smooth. Surface roughness is caused by inherent curvature of the substrates, nanoparticle modification, and fabrication defects such as particle contamination from the air. At small contacting force, the surface roughness prevents fully intimate contact between the contact electrode and the PDMS, leaving some areas untouched, as illustrated in Supplementary Figure S4. With larger force, due to elastic property, the PDMS can deform and fill more vacant space, thus leading to larger contact area. As a result, the electric output increases until all of the vacant spacing is completely filled by the PDMS, reaching a saturated limit.

Resistors were connected as external loads to further investigate the effective electric power of the NG. As demonstrated in Figure 3e, the instantaneous current drops with increasing load resistance due to Ohmic loss, while the voltage builds up. Consequently, the instantaneous power output ($W = I^2_{\text{peak}}R$) reached the maximum at a load resistance of 1 M Ω . At a contacting force of 500 N, a power output of 0.42 W was achieved (Figure 3f), corresponding to a power density of 109 W/m² for one layer of NG. This value is substantially larger than previously demonstrated ones by triboelectric nanogenerators.^{21–23} If the mechanical shaker was replaced by human footfalls which can generate a contacting force between 500 to 600 N, the maximum I_{sc} could reach up to 2 mA, as demonstrated in Figure 3g. It corresponded to an instantaneous current of 1.1 mA at a load of 1 M Ω , instantaneous output power of 1.2 W, and power density of 313 W/m². The power density can be further multiplied by stacking layers of the NGs in vertical direction. Integrating the largest I_{sc} signal (inset of Figure 3g) with time gives the maximum inductive charges of 2.3 μC that flow between the two electrodes, giving a maximum triboelectric charge density of 594.2 $\mu\text{C}/\text{m}^2$. Compared to previous works, the surface charge density represents an increase of at least 8 times.²¹ The apparent deviation shown in Figure 3g is probably caused by impact from footfall which lacks control on position, force, and direction. However, it is noted that the mean value is comparable to that obtained with the mechanical shaker (1.2 mA in Figure 3d).

As an important figure of merit, the energy conversion efficiency of the NG was calculated. The conversion efficiency is defined as the ratio between the electric energy that is delivered the load by the NG and the mechanical energy the NG possesses. Figure 4a is a current pulse output produced by human footfall at load resistance of 1 M Ω . The time span between t_1 and t_2 represents a single contact. With an external load of pure resistance, the electric energy delivered by the NG is equal to the Joule heating energy, which is presented below.

$$\begin{aligned} E_{\text{electric}} &= Q = \int_{t_1}^{t_2} I^2 \cdot R \cdot dt = R \cdot \int_{t_1}^{t_2} I^2 \cdot dt \\ &= 1 \times 10^6 (\Omega) \cdot \int_{22.7144}^{22.7200} I^2 \cdot dt = 0.74 \text{ mJ} \end{aligned} \quad (1)$$

where Q is the Joule heating energy, I is the instantaneous current, and R is the load resistance (Figure 4b). Consequently, the average power output (W_{average}) can be obtained by

$$\begin{aligned} W_{\text{average}} &= \frac{E_{\text{electric}}}{t_2 - t_1} = \frac{0.74 \text{ mJ}}{(22.7200 - 22.7144) \text{ s}} \\ &= 132.14 \text{ mW} \end{aligned}$$

As soon as the mechanical energy is introduced, it presents in two forms, that is, elastic energy stored in the springs and kinetic energy carried by a moveable substrate of the NG. The elastic energy is later released without converting into electric energy, which is calculated by

$$E_{\text{elastic}} = \frac{1}{2} \cdot k \cdot x^2 \cdot N = 2.56 \text{ mJ} \quad (2)$$

where k is the spring constant ($k = 1278.88 \text{ N/m}$), x is the displacement of a spring that is equal to the spacing between the two contacting surfaces ($x = 1 \text{ mm}$), and N is the number of springs ($N = 4$). For kinetic energy, at the moment when the

two substrates make a contact, it completely transforms to other forms, including electric energy and thermal energy. It can be calculated by the following equation.

$$E_{\text{elastic}} = \frac{1}{2} \cdot m \cdot v^2 = 4.97 \text{ mJ} \quad (3)$$

where m is the mass of the moveable substrate ($m = 13.45 \text{ g}$, the mass of gold thin film and PDMS layer are negligible), and the v is the velocity of the substrate when a contact is just about to be made ($v = 0.86 \text{ m/s}$).

Therefore, the energy conversion efficiency (η) is calculated as

$$\begin{aligned} \eta &= \frac{E_{\text{electric}}}{E_{\text{mechanical}}} \times 100\% \\ &= \frac{E_{\text{electric}}}{E_{\text{elastic}} + E_{\text{kinetic}}} \times 100\% \\ &= \frac{0.74 \text{ mJ}}{2.56 \text{ mJ} + 4.97 \text{ mJ}} = 9.8\% \end{aligned} \quad (4)$$

It is to be noted that the above result is the overall efficiency at device level. However, at conversion process level, the elastic energy stored in the springs does not participate in energy conversion. Therefore if we solely take into account the kinetic energy that actually partially converts to electric energy, the direct efficiency at conversion process level is

$$\eta_{\text{direct}} = \frac{E_{\text{electric}}}{E_{\text{kinetic}}} \times 100\% = \frac{0.74 \text{ mJ}}{4.97 \text{ mJ}} \times 100\% = 14.9\% \quad (5)$$

The superior power output of the NG enables tremendous applications, not just only for powering a single small electronics. Here we demonstrated an application of the NG on a large scale, simultaneously driving a large number of electronic devices. Arrays of commercial multicolor LED bulbs were assembled in serial to fabricate LED panels. The NG serves as a sole and direct power source for the LEDs. Triggered by human footfalls, the NG generated current pulses, instantaneously lighting up as many as 600 LED bulbs at an estimated output open circuit voltage of $\sim 1200 \text{ V}$ (Figure 4c–h). The footfalls and light emission were synchronized, indicating that the NG was a real-time power source (see Supplementary Movies 1, 2, and 3). This successful demonstration indicates other immediate applications, such as self-lighting shoes and self-lighting tiles which can be luminous upon footfalls.

The unprecedentedly high power output of the NG is mainly attributed to three reasons. First, the contact electrode plays dual roles of electrode and contacting surface. Compared to previously reported designs in which both of the contacting surfaces are made of polymers, more inductive charges will be generated for the new design (see Supporting Information for comparison between the two structures). Second, the elastic property of PDMS enables conformal contact despite of surface roughness. The PDMS can easily deform in response to small pressure and fill the otherwise vacant space that result from substrate curvature and fabrication defects. The tolerance on surface roughness ensures as much contact area as it can be possibly obtained. Last but not the least, the surface modification by gold nanoparticles plays an important role for the output enhancement. It can offer 5-fold increase on the current output compared to the device without modification

(Supplementary Figure S5), which in turn gives power enhancement of 25 times. Physically, the bumpy surface of the nanoparticle provides a larger contact area than a flat surface does. Chemically, the as-synthesized gold nanoparticles are positively charged in nature.³⁰ We suggest that the already carried positive charges can add up with triboelectric charges upon contact, leading to a largely enhanced surface charge density and thus a substantially higher electric output. Follow-up study is being conducted to systematically investigate the mechanism for the nanoparticle-enabled enhancement. Therefore, optimized structure, proper selection of materials, and functional surface modification are the three key factors that contribute to the record high power output. If we take the whole size of the NG into consideration (see Methods for detailed specifications), a volume power density as high as 54 268 W/m³ can be expected. This value reveals an extremely attractive perspective for applying the NG on a large scale.

In summary, we invented a new type of triboelectric NG that delivered an unprecedentedly high power output. Simplified structure and nanoparticle-enabled surface modification are key factors that enabled this gigantic enhancement. The maximum short-circuit current of 2.0 mA was obtained. That gives instantaneous power output of 1.2 W, power density of 313 W/m², average power output of 132.1 mW, open-circuit voltage of ~1200 V, and energy conversion efficiency of 9.8% at the device level. The NG was capable of lighting up as many as 600 commercial LED bulbs simultaneously by converting commonly ambient mechanical energy such as human footfalls. This demonstration unravels large-scale applications of the NG and broadens our horizons on the capability of the NG. With such a high power output, we envision energy harvesting by the triboelectric NG not only from human footfall but also from rolling wheels, wind power, and ocean waves.

Methods Summary. *Materials.* Hexadecyltrimethylammonium bromide (≥99%) was purchased from Sigma. Sodium tetrachloroaurate dihydrate (99%) and 1,4-benzenedithiol (99%) were purchased from Aldrich. Hydrazine hydrate solution (78–82%) was purchased from Sigma-Aldrich. Deionized water was obtained using a Milli-Q ultrapure (18.2 MΩ cm) system.

Synthesis of Gold Nanoparticles. A solution (50 mL) containing sodium tetrachloroaurate dihydrate (1 mM) and hexadecyltrimethylammonium bromide (10 mM) was brought to a vigorous boil with stirring in a round-bottom flask fitted with a reflux condenser; hydrazine hydrate solution (20 μL) was then added rapidly to the solution. The solution was heated under reflux for another 8 min, during which time its color changed from pale yellow to pale red. The solution was cooled to room temperature while stirring continuously. The average size (56 nm) of the synthesized gold nanoparticles was verified through SEM analysis.

Self-Assembly of Gold Nanoparticles onto Au Thin Film. Au films were derivatized by immersion in a solution of 1,4-benzenedithiol for 12 h and rinsed with methanol and then water. The derivatized Au films were then immersed in a solution of gold nanoparticles for 12 h to allow for complete adsorption of a single gold nanoparticle layer. Before the SEM characterization and electrical measurement, nonadsorbed gold nanoparticles were removed by rinsing with water.

Fabrication of the Triboelectric NG. To fabricate the NG, two pieces of cast acrylic glass were prepared as substrates with dimensions of 3 in. by 3 in. by 3/32 in. Four half-thorough holes were drilled at corners as houses for spring installation. 50

nm of gold were deposited on both of the substrates by e-beam evaporator (2 in. × 3 in.). On one of the substrates, fluid PDMS that consists of base and curing agent in a ratio of 5:1 was spin-coated to form a 10-μm-thick layer. Then it was cured at 100 °C for 45 min. On the other substrate, gold nanoparticles were uniformly distributed on gold surface by self-assembly. Subsequently, four springs (spring constant = 7.3 lb/inch) were installed in the houses to connect the two substrates together, leaving a spacing of 1 mm between the gold and the PDMS. The spacing is required to be substantially larger than the polymer thickness to ensure effective generation of inductive charges.^{31,32} Finally, conducting wires were connected to the two metal layers as leads for subsequent electric measurement.

■ ASSOCIATED CONTENT

📄 Supporting Information

More detailed information about experimental setup, electrical output of the NG with reversed connection to the measurement instrument, illustration of the force-dependence contact area, comparison between one-side-polymer structure with double-side-polymer structure, and electrical output of the NG without nanoparticle enhancement. This material is available free of charge via the Internet at <http://pubs.acs.org>.

■ AUTHOR INFORMATION

✉ Corresponding Author

*E-mail: zlwang@gatech.edu.

👤 Author Contributions

§These authors contributed equally to this work.

📄 Notes

The authors declare no competing financial interest.

■ ACKNOWLEDGMENTS

This work was supported by Airforce, MURI, U.S. Department of Energy, Office of Basic Energy Sciences (DE-FG02-07ER46394), NSF (CMMI 0403671), Taiwan (NSC 101-2917-I-564-029), National Institute For Materials, Japan (Agreement DTD 1 Jul. 2008), and the Knowledge Innovation Program of the Chinese Academy of Sciences (KJCX2-YW-M13). Patents have been filed based on the research presented here.

■ REFERENCES

- (1) Pelrine, R.; Kornbluh, R. D.; Eckerle, J.; Jeuck, P.; Oh, S.; Pei, Q.; Stanford, S. *Proc. SPIE* **2001**, 4329, 148–156.
- (2) Miao, P.; Mitcheson, P. D.; Holmes, A. S.; Yeatman, E. M.; Green, T. C.; Stark, B. H. *Microsyst. Technol.* **2006**, 12, 1079–1083.
- (3) Round, S.; Wright, R. K.; Rabaey, J. *Comput. Commun.* **2003**, 26, 1131–1144.
- (4) Jeon, Y. B.; Sood, R.; Jeong, J.-h.; Kim, S.-G. *Sens. Actuators A* **2005**, 122, 16–22.
- (5) Wang, Z. L.; Song, J. H. *Science* **2006**, 312, 242–246.
- (6) Wang, X. D.; Song, J. H.; Liu, J.; Wang, Z. L. *Science* **2007**, 316, 102–105.
- (7) Sari, I.; Balkan, T.; Kulah, H. *Sens. Actuators A* **2008**, 145–146, 405–413.
- (8) Beeby, S. P.; Torah, R. N.; Tudor, M. J.; Glynne-Jones, P.; O'Donnell, T.; Saha, C. R.; Roy, S. J. *Micromech. Microeng.* **2007**, 17, 1257–1265.
- (9) Wang, Z. L. *Sci. Am.* **2008**, 298, 82–87.
- (10) Wang, Z. L. *Adv. Mater.* **2011**, 24, 279–284.
- (11) Vullers, R. J. M.; Schaijk, R. V.; Doms, I.; Hoof, C. V.; Mertens, R. *Solid-State Electron.* **2009**, 53, 684–693.

- (12) Beeby, S. P.; Tudor, M. J.; White, N. M. *Meas. Sci. Technol.* **2006**, *17*, 175–195.
- (13) Roundy, S.; Steingart, D.; Frechette, L.; Wright, P.; Rabaey, J. *Lect. Notes Comput. Sci.* **2004**, *920*, 1–17.
- (14) Lee, M.; Bae, J.; Lee, J.; Lee, C.-S.; Hong, S.; Wang, Z. L. *Energy Environ. Sci.* **2011**, *4*, 3359–3363.
- (15) Li, Z.; Zhu, G.; Yang, R.; Wang, A. C.; Wang, Z. L. *Adv. Mater.* **2010**, *22*, 2534–2537.
- (16) Zhu, G.; Wang, A. C.; Liu, Y.; Zhou, Y.; Wang, Z. L. *Nano Lett.* **2012**, *12*, 3086–3090.
- (17) Paradiso, J. A.; Starner, T. *IEEE Pervasive Comput.* **2005**, *4*, 18–27.
- (18) Guang, Z.; Yang, R.; Wang, S.; Wang, Z. L. *Nano Lett.* **2010**, *10*, 3151–3155.
- (19) Slade, J. R.; Bowman, J.; Kornbluh, R. *Proc. SPIE* **2012**, 8383, 83830R1–83830R12.
- (20) Chiba, S.; Waki, M.; Kornbluh, R.; Pelrine, R. *Proc. SPIE* **2008**, 6927, 6927151–6927159.
- (21) Kornbluh, R. D.; Pelrine, R.; Prahlad, H.; Wong-Foy, A.; McCoy, B.; Kim, S.; Eckerle, J.; Low, T. *Proc. SPIE* **2011**, 7976, 7976051–79760519.
- (22) Zhu, G.; Pan, C.; Guo, W.; Chen, C.-Y.; Zhou, Y.; Yu, R.; Wang, Z. L. *Nano Lett.* **2012**, *12*, 4960–4965.
- (23) Fan, F. R.; Tian, Z. Q.; Wang, Z. L. *Nano Energy* **2012**, *1*, 328–334.
- (24) Fan, F.-R.; Lin, L.; Zhu, G.; Wu, W.; Zhang, R.; Wang, Z. L. *Nano Lett.* **2012**, *12*, 3109–3114.
- (25) Castle, G. S. P. *J. Electrostatics* **1997**, *40–41*, 13–20.
- (26) Nemeth, E.; Albrecht, V.; Schubert, G.; Simon, F. *J. Electrostatics* **2003**, *58*, 3–16.
- (27) Lungu, M. *Miner. Eng.* **2004**, *17*, 69–75.
- (28) Lee, L. H. *J. Electrostatics* **1994**, *32*, 1–29.
- (29) Watson, P. K.; Yu, Z. Z. *J. Electrostatics* **1997**, *40–41*, 67–72.
- (30) Saurenbach, F.; Wollmann, D.; Terris, B. D.; Diaz, A. F. *Langmuir* **1992**, *8*, 1199–1203.
- (31) Whitesides, G. M.; McCarty, L. S. *Angew. Chem., Int. Ed.* **2008**, *47*, 2188–2207.
- (32) Wang, S.; Lin, L.; Wang, Z. L. *Nano Lett.* **2012**, *12*, 6339–6346.